Geomorphology 440 (2023) 108883

Contents lists available at ScienceDirect

Geomorphology

journal homepage: www.journals.elsevier.com/geomorphology

# Coastal boulder movement on a rocky shoreline in northwest Ireland from repeat UAV surveys using Structure from Motion photogrammetry

Jasper Knight [a,*], Helene Burningham [b], David Griffiths [c], Yao Yao [b]

[a] School of Geography, Archaeology & Environmental Studies, University of the Witwatersrand, Johannesburg 2050, South Africa
[b] Department of Geography, UCL, Gower Street, London WC1E 6BT, UK
[c] Department of Civil, Environmental and Geomatic Engineering, UCL, Gower Street, London WC1E 6BT, UK

ARTICLE INFO

*Keywords:*
Boulder dynamics
Ireland
Rocky shoreline
Structure from Motion
UAV surveys
Wave climate

ABSTRACT

The degree of boulder mobility in response to coastal storms likely varies spatially and temporally along rocky shorelines, but this is difficult to evaluate from field monitoring of individual boulders alone. Structure from Motion (SfM) photogrammetry can be used to analyse changes in shoreline geomorphology or boulder distributions over time and space from rocky shorelines. This study employs data from repeated Unpiloted Aerial Vehicle (UAV) surveys in 2017, 2018, 2019 and 2022 along a 1-km stretch of a rocky shoreline in northwest Ireland. SfM techniques were used to generate orthomosaics of the bedrock platform surface from which distributions and transport patterns of boulders were examined. Based on the identification of specific boulders that appear in images from successive time slices, 16–32 % of boulders had remained stationary (had either rotated or flipped on the spot, but experienced no change in boulder position), 18–39 % had moved but less than the calculated Root Mean Square Error (RMSE) value of 23 cm, and 29–66 % of boulders had moved greater than the RMSE value, and <29 m distance in one case. In addition, a significant minority of boulders also appeared or disappeared (3–23 %) between successive time slices, which may reflect their episodic transport to/from the sea or beyond the region of interest. Overall, the results indicate that boulder movement is highly variable over time and space and does not appear to correspond with episodic wave forcing. This is different to previous studies that have described a simple deterministic relationship between boulder movement and singular wave forcing events such as storms. Repeated UAV surveys provide a consistent methodology for understanding rocky shoreline and boulder dynamics, and can offer insight into shoreline sensitivity to regional wave climate operating under more normal or 'average' conditions.

## 1. Introduction

Structure from Motion (SfM) photogrammetry is a commonly used technique for geomorphological analysis (Westoby et al., 2012; Lin et al., 2019; Rowley et al., 2020; Bonasera et al., 2022; Casella et al., 2022). It is based on the visualisation and analysis of closely-spaced digital point clouds derived remotely, from an Unpiloted Aerial Vehicle (UAV) or drone, from a flown LiDAR platform, or from a terrestrial laser scanning (TLS) instrument. The point cloud can be used to reconstruct an orthomosaic aerial image and a Digital Surface Model (DSM) of the visualised area of interest. Repeated surveys of the same area when georectified to ground control points (GCPs) can map and quantify changes in the land surface over time through calculation of the DEM of Difference (DoD), which refers to the elevational differences between the same points (either measured or interpolated) of successive surveys. An increase in elevation reflects net deposition in the environment, which may be along a beach, dune, shore platform or river floodplain, whereas a decrease in elevation reflects net erosion from this environment. This can then be used to calculate rates of change per unit time, and areal sediment budgets (e.g., Clark et al., 2021; Carvalho and Reef, 2022; Minervino Amodio et al., 2022). The SfM technique has been used in particular in environments where the land surface is clearly exposed (i.e., unvegetated), topography is relatively subdued, and where there is therefore the potential for lower vertical error when interpolating between data points (Mancini et al., 2013; Papakonstantinou et al., 2016; Rodarmel et al., 2019). Along coasts, SfM has been used to map and examine the dynamics over time and space of sandy beaches (Guisado-Pintado et al., 2019; Pagán et al., 2019;

* Corresponding author.
*E-mail address:* jasper.knight@wits.ac.za (J. Knight).

https://doi.org/10.1016/j.geomorph.2023.108883
Received 23 June 2023; Received in revised form 23 August 2023; Accepted 23 August 2023
Available online 24 August 2023

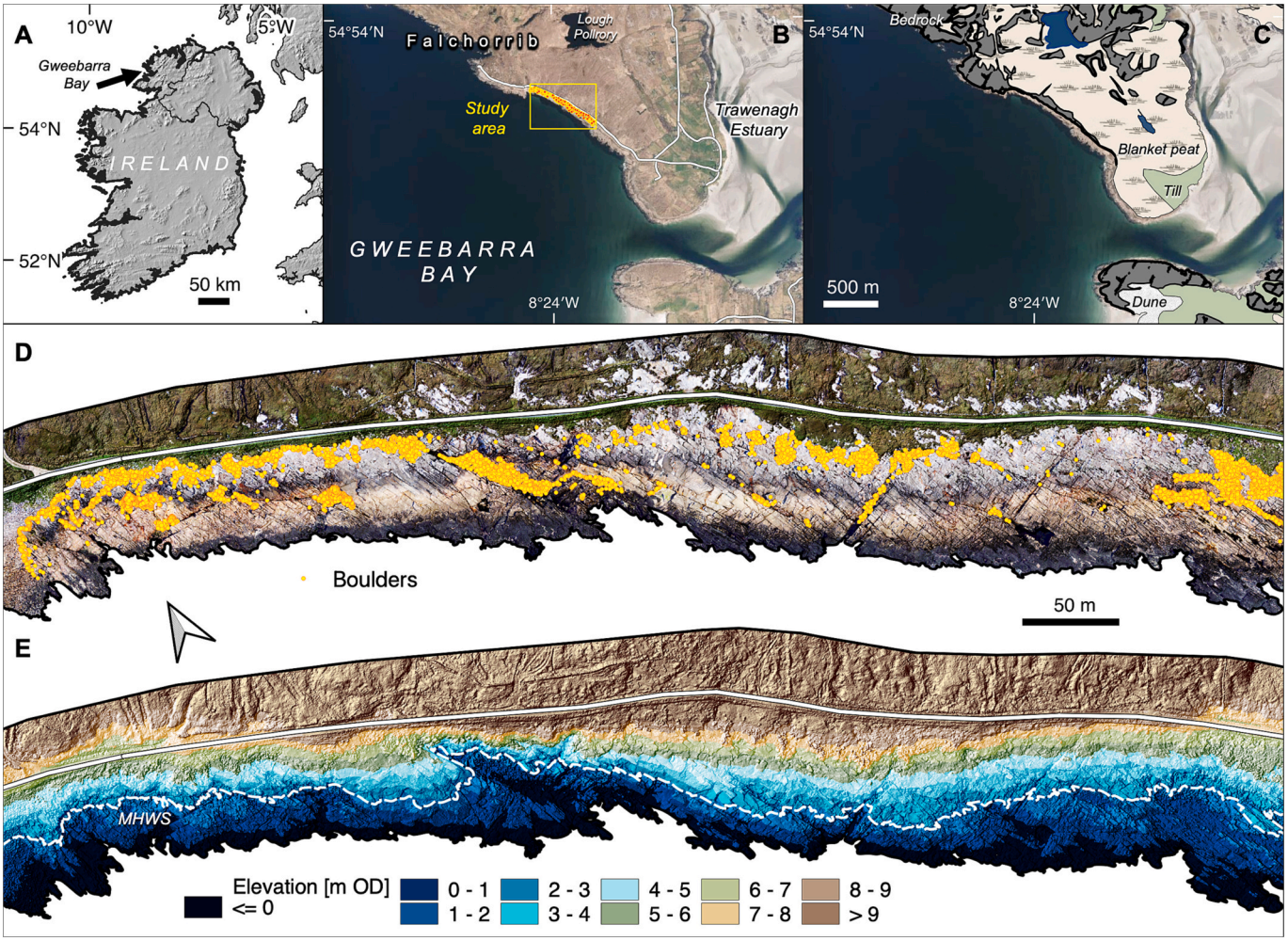


**Fig. 1.** Location and geomorphology of the study area in northwest Ireland. (A, B) Location of the study area of the rocky shoreline on the margin of Gweebarra Bay. The shoreline area of interest examined in this study is shown in the yellow box, (C) land surface composition in the study area, (D) composite UAV image showing the location of platform-attached boulders (n = 5860), and (E) processed DSM of the studied shoreline. MHWS = position of mean high water spring tide.

Carvalho et al., 2020), rock and soft-sediment cliffs (Warrick et al., 2017; Del Río et al., 2020; Gómez-Pazo et al., 2021), rock shore platforms (Swirad et al., 2019; Yuan et al., 2022), and boulder shorelines and boulder movement (Boesl et al., 2020; Nagle-McNaughton and Cox, 2020; Sedrati et al., 2022).

SfM is particularly useful on rocky shorelines where surfaces are eroded via the detachment of discrete blocks of rock; these discrete changes are easily resolvable against a wider bedrock surface that remains broadly unchanged, and in so doing, the position of boulders along rocky shorelines can be mapped. Coastal boulder mapping has been undertaken at many different field sites globally, especially along high storm wave-energy coasts where boulders are particularly mobile such as in Italy (Barbano et al., 2010; Delle Rose et al., 2021), western Iberia (Pérez-Alberti and Trenhaile, 2015; Gómez-Pazo et al., 2019; Oliveira et al., 2020), Iceland (Autret et al., 2023), Ireland (Scheffers et al., 2010; Knight and Burningham, 2011; Cox et al., 2012, 2018; Erdmann et al., 2018) and western France (Autret et al., 2016, 2018). Throughout, there has been an emphasis on the role of energetic wave regimes in boulder dynamics, hence many studies have compared the rates or direction/amount of boulder movement to forcing by individual storm or tsunami events (e.g., Autret et al., 2016; Naylor et al., 2016; Erdmann et al., 2018; Delle Rose et al., 2021). Although not incorrect, this deterministic relationship requires critical examination because coastal boulders may be mobile under a range of wave conditions, not just those related to storm or high energy events.

Although SfM is an effective tool to map and monitor boulder movement across rocky shorelines and has been used in several studies (e.g., Autret et al., 2016; Boesl et al., 2020; Nagle-McNaughton and Cox, 2020; Sedrati et al., 2022), there are some limitations of this approach (Yao et al., 2023). Limitations are that: (1) Individual boulders may move onshore or offshore and so they may not be present on successive surveys; (2) if a boulder overturns (flips) or rotates then their plan-view outline shape may change between successive surveys, and this can cause uncertainty in their automated extraction and mapping; (3) even if specific boulders can be identified on successive surveys, the straight-line net movement (length, direction) calculated from these surveys may not reflect their true paths or the episodic nature of their movement. Real-time transport styles, patterns and rates are therefore uncertain; and (4) the relationships of boulder movement to wave forcing or to individual storm events are not clear, and there may be low predictability of potential boulder movement based on wave energy (derived from the significant wave height $H_s$), shoreface slope and boulder mass alone, as described by the commonly-used Nott equation (Nott, 2003; see Cox et al., 2020 for discussion). In addition, it is likely that shoreline boulder deposits exposed to different wave/storm climates and with varied geological controls will show different patterns of wave response. This can also limit the predictability of boulder movement in wave-forced systems.

The aim of this study is to evaluate boulder dynamics along a rocky shoreline in northwest Ireland using data from repeated UAV surveys

**Fig. 2.** View seaward of a wave-exploited channel developed along a line of structural weakness within the intertidal zone. The base of the channel is floored with loose boulders.

(conducted in 2017, 2018, 2019 and 2022). SfM techniques were used to derive orthomosaics, DSMs and to map and track the trajectories of individual boulders between successive time slices. The results of this analysis show that boulder movement is highly variable over time and space and that, unlike many previous studies, there is not a simple deterministic response of boulders to wave or storm forcing. Throughout, the generic term *boulder* is used to describe all detached bedrock-derived clasts located along the rocky shoreline, irrespective of their size.

## 2. Study area

The study area is in northwest Ireland (Fig. 1). This region is mesotidal (3.5 m tidal range) with offshore $H_s$ of 2.9 m, reaching >8 m during the winter season but with considerable variability. Boulder dynamics along the rocky west coast of Ireland have been examined in several studies (e.g., Scheffers et al., 2009; Cox et al., 2018; Erdmann et al., 2018; Van Blunk et al., 2021). These have demonstrated that boulders of different sizes, including megaclasts of 40–80 t in mass, can be moved both horizontally across-shore and vertically by extreme storm waves (Cox et al., 2012) as well as by more common winter storms (Knight and Burningham, 2011). Most of these studies have been based on the Carboniferous limestone shorelines of the central Ireland coast where the bedrock breaks into large, geologically-controlled slabs and blades (sensu Zingg, 1935) that are prone to hydraulic jacking and flipping (e.g., Herterich et al., 2018; Cooper et al., 2019). However, along the northwestern Ireland coast granite shorelines with regular fracture sets are present where bedrock breaks into blocks that are more equant in shape (Knight et al., 2009; Knight and Burningham, 2011). These blocks experience very different hydrodynamic behaviours, with sliding and rolling dominant. This means that the boundary conditions (bedrock structures, values of $H_s$) influencing boulder mobility are quite different and these studies on boulder dynamics cannot be uncritically compared even though they are in the same region and subject to the same broad regional wave regime.

Bedrock in the study area comprises Trawenagh Bay biotite granite which is a coarse grained rock with multiple and intersecting contraction joints that vary in orientation around the batholith (Long and McConnell, 1999; Stevenson et al., 2006; Stevenson, 2009). The granite batholith was emplaced during the late Caledonian Orogeny in the middle Devonian (Long and McConnell, 1999). Along the study shoreline, bedrock fractures are oriented dominantly at 155–335° and subordinately at 070–250°, and these act as lines of weakness for weathering and wave processes. The shoreline examined by UAV survey in this study is located on the south-facing margin of Gweebarra Bay, northwest Ireland, seaward of the Trawenagh estuary, County Donegal (Fig. 1). The bedrock shoreline in total is 1.2 km long, 30–60 m in width, linear, and faces southwest towards the open Atlantic. Glacially-eroded bedrock hills rise to the north of the site; to the south the bedrock surface is of low relief (Knight, 2009) where the bedrock shoreline itself extends from subtidal to supra-littoral, reaching a maximum elevation of around 10 m asl (Fig. 1E). Prominent and discrete boulder ridges have been identified along the landward fringe of the bedrock shoreline, reflecting the accumulation of loose boulders that have been detached by waves from the shore platform (Knight and Burningham, 2011). Previous UAV surveys have shown that boulders along this coastline can be quantified and automatically extracted using SfM techniques, enabling gross estimations of the number of mobile boulders, but also highlighted the challenges involved in tracking individual boulders between successive surveys (Yao et al., 2023). The focus here is the latter, and therefore the analyses followed a manual digitising process to ensure confident re-identification of moving boulders.

## 3. Methods

A UAV and a differential GPS (dGPS) system were used to obtain aerial imagery and ground control point (GCP) data (3D coordinates) of the study area in September 2017, May 2018, May 2019, and May 2022. GCPs (47 in total) and checkpoints were acquired using a Leica GS15 rover connected to a 1200 reference station, and included both temporary ground marker flags and natural bedrock surface features that remained unchanged throughout the surveys. Positions were referenced to UTM Zone 29 N (EPSG: 32629) via a geodetic benchmark belonging to the Ordnance Survey of Ireland located near the jetty at the northwest end of the study area. Coordinate quality of the dGPS-acquired points was 0.77 cm in the horizontal and 1.11 cm in the vertical.

UAV images were obtained using a DJI Phantom 4 Pro comprising a built-in RGB camera with a 1" CMOS sensor acquiring 20 MP images, commonly used in geomorphological surveys (e.g., Biolchi et al., 2019; Boesl et al., 2020; Gallo et al., 2021). Flight plans were focused on a core set of nadir images obtained along flightlines parallel to the shoreline, where image overlap was set to at least 80 % front overlap and 60 % side overlap; flight height was around 120 m above the ground, achieving a ground sampling distance of 2–3 cm. Surveys undertaken in 2018 and 2019 were supplemented with oblique images along non-parallel flightlines: 308 images in total were acquired in 2017, 933 images in 2018, 504 images in 2019, and 242 images in 2022. The mapped shoreline was 1 km long in total, excluding the extreme northwest end, which transitioned into a boulder and then sandy beach and the southeast end, which entered a boulder-filled embayment.

UAV images and control point coordinates for each survey year were processed using Agisoft PhotoScanPro (v1.3.0) following a common workflow of aligning photos, importing GCPs, and optimizing cameras, to achieve a good accuracy followed by point cloud and orthomosaic construction (e.g., Brunier et al., 2016). Control points delivered cm-level accuracy: Root Mean Square Error (RMSE) in the GCPs ranged


**Fig. 3.** The varied morphology of the studied rocky shoreline. (A) The rock platform with boulder ridges, (B) the stepped profile of the rock platform, caused by the intersection of bedrock joints, (C) dissociation of boulders along the joints of the platform, note the isolated boulders sitting on the rock surface, (D) wave-rounded boulders contained within a bedrock depression within the lower part of the tidal frame.

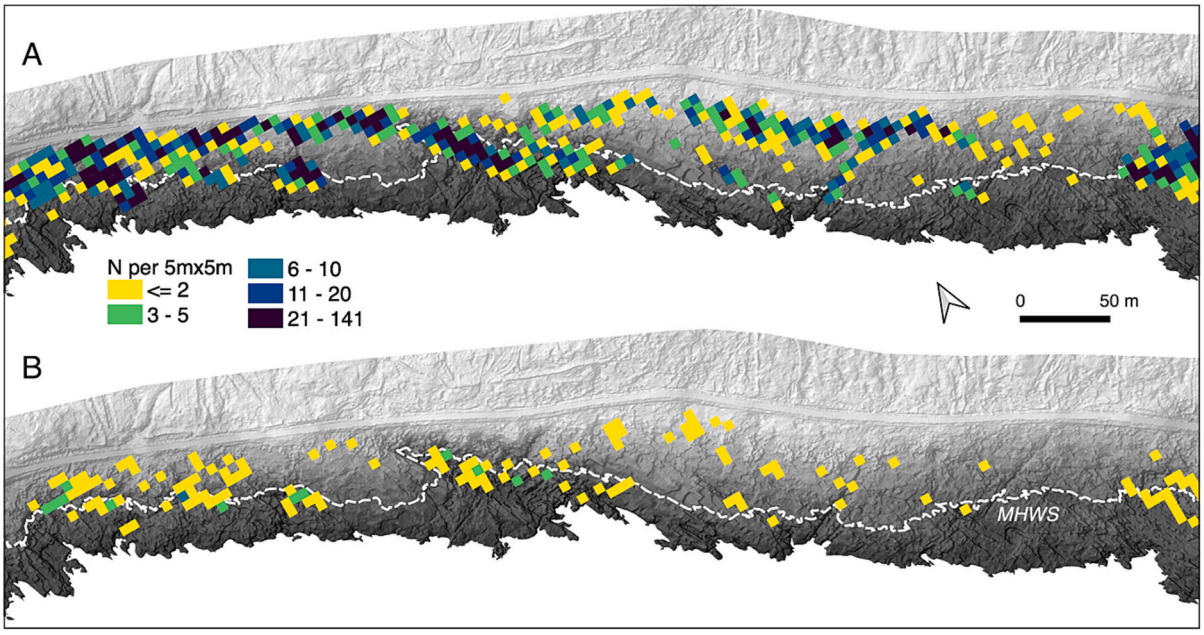


**Fig. 4.** Map of boulder density (in 5 × 5 m cells) across the platform, for (A) all platform-based boulders present in the May 2022 imagery (n = 5860) and (B) the number of boulders that moved between 2019 and 2022.

**Table 1**
Results of boulder movement analysis between successive time periods in the UAV survey.

| | 2017–18 | 2018–19 | 2019–22 |
|---|---|---|---|
| Number of boulders present on both images | 268 | 300 | 243 |
| *Boulder travel:* | | | |
| Stationary boulders recording zero travel (% of total) | 35 (13 %) | 144 (48 %) | 47 (19 %) |
| Boulders with travel >0 cm, but <23 cm (SfM reconstruction RMSE) | 80 (30 %) | 67 (22 %) | 36 (15 %) |
| Total number of statistically stationary boulders | 102 (38 %) | 58 (19 %) | 93 (38 %) |
| Boulders recording movement between 23 cm and 1 m | 51 (19 %) | 31 (10 %) | 67 (28 %) |
| Boulders recording travel >1 m | 153 (57 %) | 89 (30 %) | 160 (66 %) |
| Total number of boulders that moved >23 cm | 35 (13 %) | 144 (48 %) | 47 (19 %) |
| Largest distances travelled by boulders | Two boulders moved >14 m | One boulder moved 20 m, one 22 m | One boulder moved 15 m, one 29 m |
| Of those that travelled: | | | |
| 50th percentile distance | 0.76 m | 0.61 m | 0.82 m |
| 75th percentile distance | 1.4 m | 1.74 m | 1.98 m |
| 95th percentile distance | 5.5 m | 10.82 m | 5.79 m |
| *Movement style of boulders that travelled:* | | | |
| Rotation (% of those that travelled) | 76 (50 %) | 57 (64 %) | 124 (78 %) |
| Flipping (% of those that travelled) | 43 (28 %) | 25 (28 %) | 48 (30 %) |
| Both rotation and flipping (% of those that travelled) | 32 (21 %) | 19 (21 %) | 40 (25 %) |
| Boulder movement by neither rotation nor flipping (i.e., by translation) | 66 (43 %) | 26 (29 %) | 28 (18 %) |
| *Movement style of boulders that were statistically stationary:* | | | |
| Rotation (% of total that were statistically stationary) | 32 (28 %) | 44 (15 %) | 21 (9 %) |
| Flipping (% of total that were statistically stationary) | 1 (0 %) | 5 (2 %) | 4 (2 %) |
| Both rotation and flipping (% of total that were statistically stationary) | 0 (0 %) | 0 (0 %) | 3 (1 %) |
| Number of boulders that did not move at all in this time frame, but did move within another period | 82 (31 %) | 162 (54 %) | 61 (25 %) |
| *Change in boulder populations:* | | | |
| Disappeared from the first time period to the second | 26 (9 %) | 42 (12 %) | 69 (22 %) |
| Appeared from the first time period to the second | 74 (22 %) | 12 (4 %) | 13 (5 %) |
| Net change in boulder numbers through disappearance/appearance | +48 | −30 | −56 |

across 0.03 m (2017), 0.05 m (2018) and 0.06 m (2019, 2022). Check point accuracy was more variable, with a RMSE of 0.23 m, and this value was used to identify whether a boulder had moved position relative to stationary boulders (see Section 4.2). Following this, individual unique boulders were identified and mapped for each time period across the rock platform. The methodological approach for doing this was relatively pragmatic and this is because individual and isolated boulders are more easily identified on the planar rock platform whereas the morphology of boulders that are clustered together within bedrock depressions is not always resolvable where they are partly hidden by other boulders. Boulders were included in the study where the boulder outline was clearly visible and not obscured by other boulders. In addition, no specific minimum size of boulders was used but, based on the RMSE, all boulders identified and quantified in this survey were greater than ~30 cm diameter. Each boulder that was clearly identified within the spatial frame of interest was assigned a unique identifier code. The outline of each unique boulder was digitised, and from this polygon the axial lengths of the boulder, and its area and perimeter could be calculated. Note that boulder volume (area x height) was not calculated in this study. The outline shape of the boulder was used as a template to evaluate whether the boulder had rotated in angle relative to the shoreline (here termed *rotation*) or been overturned (here termed *flipped*) between successive time slices. The centroid position (*x,y*) of this polygon was then used to calculate (1) the distance moved (in m) by the centroid of the boulder in the (*x,y*) frame between the successive time slices, and (2) the linear trajectory (in direction relative to true north) of the centroid of the boulder between the time slices. If the boulder centroid was within the RMSE of its previous position, it was deemed to have not moved position between successive time slices, here termed *stationary*, even if it had rotated or flipped. Changes in the position of any boulder can only be calculated where it can be identified at successive time slices (i.e., for the time periods of 2017–18, 2018–19, 2019–22), and this is a limitation of this study if the boulder disappears or is not identified at any one time slice. For this reason, therefore, the number of boulders mapped at any one time slice and the number of boulders moved between successive time slices is highly variable. The aggregated results across all of the boulders analysed, across the shore platform and for the different time slices examined, are compared qualitatively with the offshore wave climate extracted from ERA5 reanalysis data in order to more critically examine the nature of wave forcing and boulder dynamic response.

## 4. Results and interpretation

### 4.1. Rocky shoreline geomorphology and boulder distributions

The UAV surveys clearly reveal the bedrock structural features along the studied shoreline. Intersecting contraction joints in the granite bedrock are clearly resolved and influence the location and orientation of small-scale channels and depressions (Fig. 1D, E). Erosional exploitation of these lines of structural weakness have developed narrow and linear channels (2–4 m wide, <5 m deep) that are as long as the extent of the intertidal zone is wide. These channels widen in a seaward direction where they respond to higher wave energy and inundation at lower points in the tidal frame (Fig. 2). The floors of these channels and depressions are covered with a litter of boulders several boulders thick, some of which may have accumulated through in situ weathering or block detachment within the depression, but based on their sub-rounded and sub-angular shapes, most are probably derived by wave transport of individual boulders into the depression from the shoreface, or from boulders being washed into the depression from the flatter and higher-elevation platform surfaces above. Thus, these channels and depressions represent locations of net boulder capture and their high and steep sides likely preclude boulders being lost from the channels except directly seawards. The UAV data also identify the macroscale morphology of the shore platform. On steeper parts of the platform and in more seaward positions, the bedrock surface commonly has a stepped profile 15–50 cm high, indicative of hydraulic jacking (plucking) of joint-defined boulders from rockhead (e.g., Hastie et al., 2021) (Fig. 3).

Mapped boulder distributions across the studied shoreline are highly variable (Fig. 4A). Boulders contained within bedrock depressions and channels are considered to have low mobility because they are laterally constrained within topographic lows and are closely packed against surrounding boulders. Boulders are also stacked within relatively immobile boulder ridges located in the upper intertidal and supratidal zone of the platform (Knight and Burningham, 2011) and it is this latter concentration in particular that is shown in Fig. 4A. These immobile boulders represent some ~90 % of the total boulder population. The spatially-aggregated distribution of the mobile boulder population mapped on the UAV survey is shown in Fig. 4B. This distribution highlights that there are no particular patterns to boulder distributions and

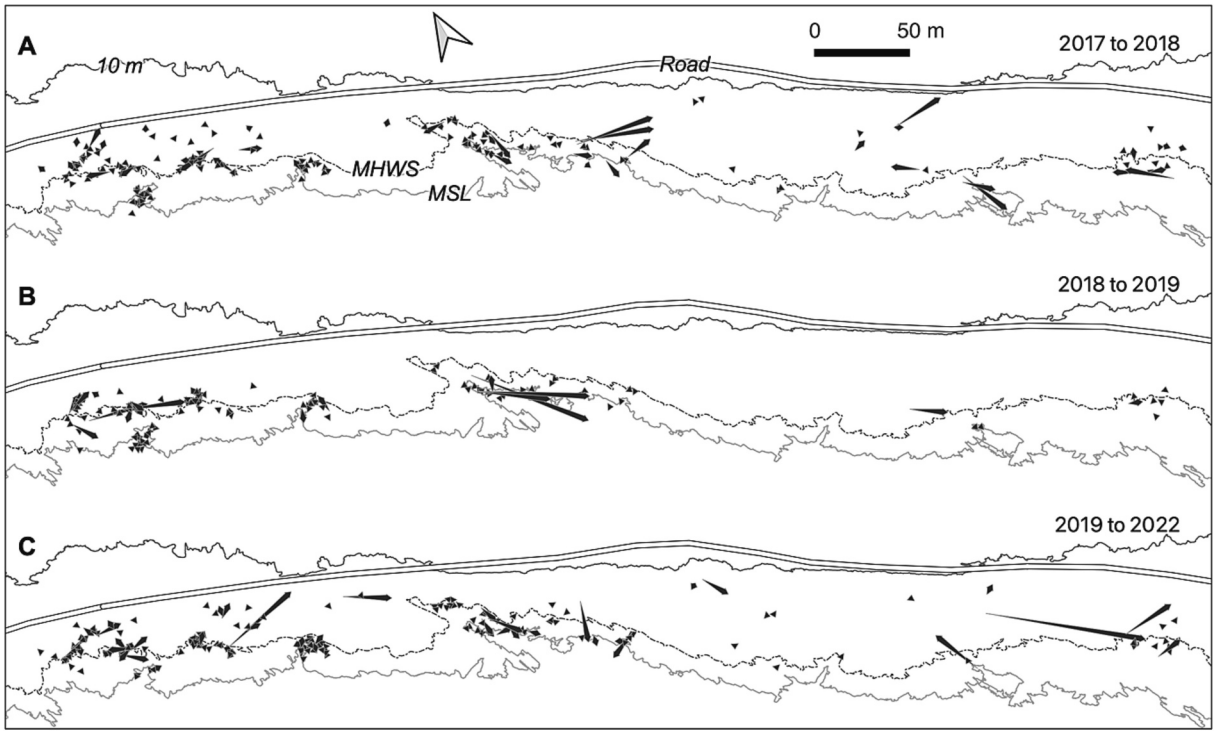


**Fig. 5.** Movement vectors for all boulders mapped in the periods 2017–18, 2018–19 and 2019–22. Note the arrow scale is exaggerated by a factor of three for visualisation purposes. MHWS = position of mean high water spring tide. MSL = mean sea-level position.

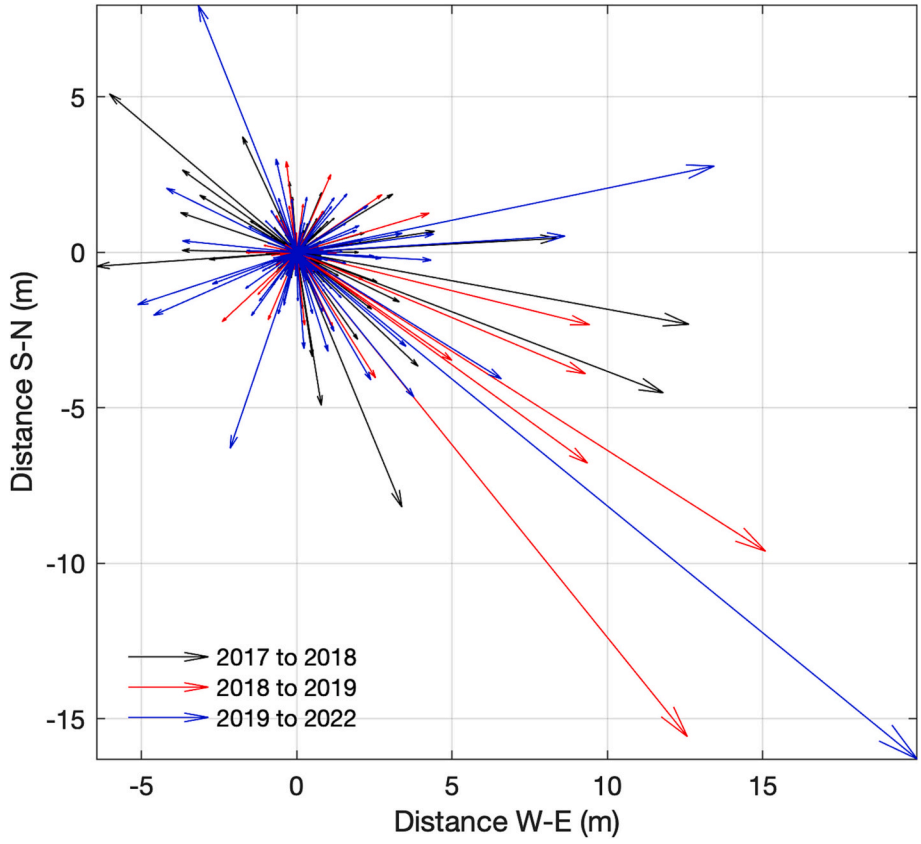


**Fig. 6.** Net movement vectors for all boulders across the different time periods, from a (*0,0*) origin.

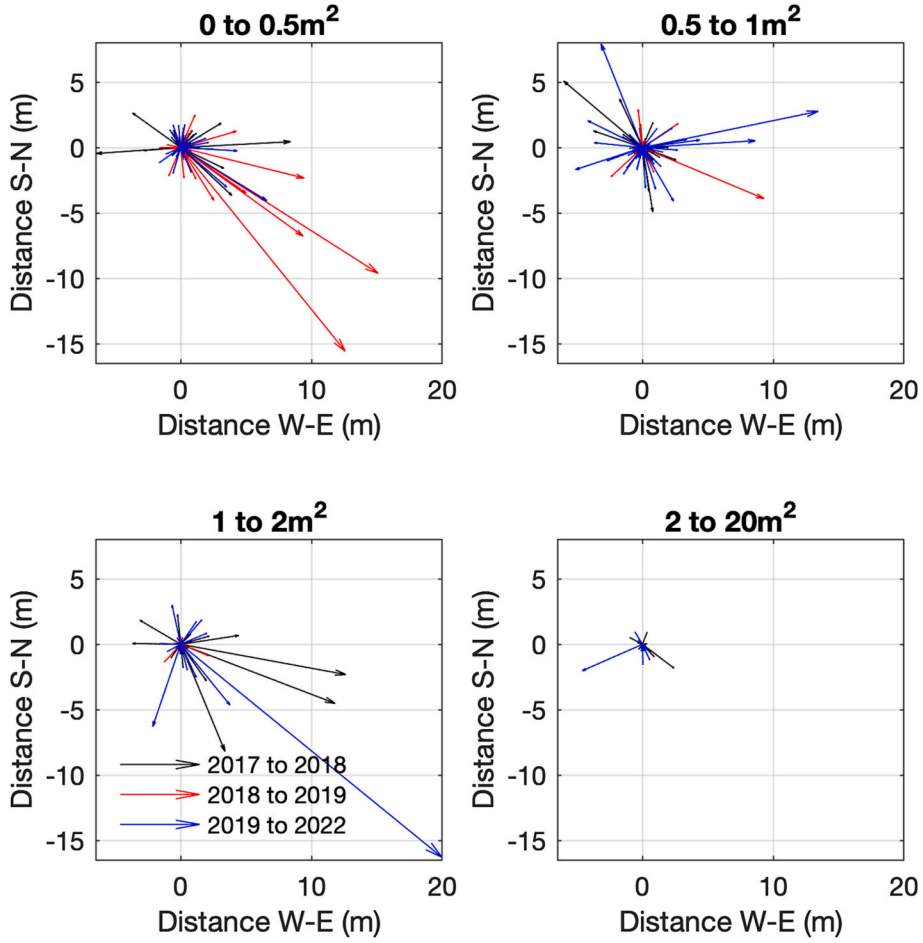


**Fig. 7.** Movement vectors separated based on boulder size across the different time periods, from a (*0,0*) origin.

therefore mobility but it can be seen that boulders are often located along structural lineaments developed in the underlying granite, which can be clearly identified on the DSM of the platform surface (Figs. 1D, 4). This may suggest locations where structural control influences the extent and power of wave run-up, and the deposition, trapping, and accumulation of boulders.

### 4.2. Boulder dynamics over time and space

In total, 392 unique boulders making up the mobile population were identified in this study. Not all boulders were identified on each image: 294 were present and mapped in 2017, 342 in 2018, 312 in 2019, and 256 in 2022. Of these 392 boulders, 79 (20 %) were identified only on one of the four images, 30 (8 %) on two images, 67 (17 %) on three images, and 216 (55 %) on all four images. Where present on successive images, boulder movement can be assessed in terms of (1) the direction and distance of travel, and (2) the style of movement (rotation or flipping). It should be noted that some boulders may have travelled but not rotated/flipped, and some boulders that have not travelled (i.e., remained stationary) may nonetheless have rotated/flipped. All boulders that showed any travel or movement between 2017 and 2022 were mapped for each survey. A detailed explanation of boulder movement patterns for the time period 2017–18 is now described. Note that this explanation is not repeated for the periods 2018–19 and 2019–22 which are instead presented in Table 1 only, with the data rows listed in the order in which they are described in the following paragraph.

For the period 2017–18, 268 individual boulders are present on both images. Of these, 35 (13 %) recorded zero travel, and 80 (30 %) recorded a movement of between zero and the RMSE value of 23 cm. These boulders are then considered to be statistically stationary, which accounted for 43 % (n = 115) of boulders in 2017–18 in comparison to a total of 153 boulders (57 %) statistically travelling. Distances of between 23 cm and 1 m were recorded by 102 boulders (38 %), and a further 51 boulders (19 %) moved >1 m. Two boulders recorded a distance travelled of over 14 m. The 50th, 75th and 95th percentile distances moved were 0.76 m, 1.4 m, and 5.5 m respectively. Of those boulders that moved further than 23 cm 76 (50 %) rotated, 43 (28 %) flipped, 32 (21 %) did both and 66 (43 %) did neither (i.e., only direct lateral movement (translation) across the platform). Of the boulders that were statistically stationary, 32 rotated (28 %) and one (<1 %) flipped. This leaves 82 boulders (31 %) that did not move at all between 2017 and 2018, but then moved at some point between 2018 and 2022. Of the boulders that were present in 2017 (n = 294), 26 of these (9 %) were not seen on the 2018 image, giving a 'disappearance' value of 9 %. However, 74 boulders that were not present on the 2017 image were present on the 2018 image, giving an 'appearance' value relative to the total 2018 boulder population (n = 342) of 22 %, and a net gain of 48 boulders. This style of analysis was repeated for the periods 2018–19 and 2019–22, as is recorded in Table 1.

Across the three successive time periods, the aggregated results of boulder dynamics show some interesting differences and similarities. The periods 2017–18 and 2019–22 have very similar proportions of boulders moving but in the latter period there was a very high proportion of rotation in travelling boulders. Rotation appears to be around twice as common a style of boulder movement than flipping across all periods but lateral translation (travel) is the most common form of movement. The period 2018–19 had a much lower overall proportion of boulder movement, but the 75th percentile distance moved was greater


**Fig. 8.** Boulder movement (indicated with red lines) from one time-step to another, around boulder ridges (marked in the 2018 image). Boulder A has an area of 0.76 $m^2$, and travelled a gross distance of 2.28 m, and a net distance (2017 to 2022) of 1.18 m. Boulder B has an area of 0.6 $m^2$, and travelled a gross distance of 6.15 m and a net distance of 5.53 m.

than in the other time frames, and included two boulders that moved >20 m. Although appearing/disappearing boulders may be difficult to characterise, with a lack of clarity around whether they are lost from the region of interest, or simply not identifiable, it is notable that of the 392 boulders identified in total, 25 (6 %) were only recorded in 2017, 31 (8 %) only in 2018, 11 (3 %) only in 2019, and 12 (3 %) only in 2022. No boulder appeared or disappeared more than once. The phenomenon of boulder appearance/disappearance has not been fully described before.

Spatial analysis of travelling boulders in the three time periods is shown in Fig. 5, which shows that lateral movement takes place in the locations of highest boulder density outlined in Fig. 4, and around the position of MHWS. There is high variability in the magnitude and direction of boulder transport paths both between different time periods and across the shoreline in each time period. Distances travelled do not appear to have any specific spatial association, with large distances evidence across the entire region comprising mobile boulders. However, it is notable that boulder transport takes place in particular along structurally-controlled channels where wave energy becomes focused. In detail, integrating evidence of all boulder movements in different time periods shows a predominance of southeasterly transport vectors (Fig. 6) but there is high variability to this general pattern. The resultant vector (not shown) for 2017–18 is towards the east-southeast whereas for 2018–19 it is more southeasterly and for 2019–22 it is far more scattered.

Based on the polygons of boulder outlines extracted from the UAV imagery, boulder size can be inferred from polygon area, perimeter and size of the major and minor axes. Analysis of movement vectors based on boulder planform area is shown in Fig. 7. This shows that smaller boulders are generally more mobile that larger ones, consistent with the literature (e.g., Bressan et al., 2018; Brayne et al., 2020), but that this varies considerably and in different time periods. For example, boulder movement in 2018–19 mostly gave rise to transport of small boulders to the southeast, whereas in 2019–22 larger boulders moved and in a wider range of directions.

In more detail, the specific nature and dynamics of boulders at a very local scale can be gained through examination of sequential UAV images from the same location. An example is patterns of discrete boulder movement around boulder ridges that are present above MHWS at different locations across the platform (Knight and Burningham, 2011) (Fig. 8). Here, the boulder ridges themselves are relatively immobile features because of their stacked and imbricated nature, with limited movement of only a few boulders on the seaward fringe of the ridges. There is very limited movement of two single boulders in the period 2017–18, no movement at all in 2018–19, and movement of the same two boulders in 2019–22; the distance moved was greater in 2019–22 than in 2017–18.

On the rock platform surface, different patterns are observed (Fig. 9). This sector of the shoreline is more variable in boulder movement, with

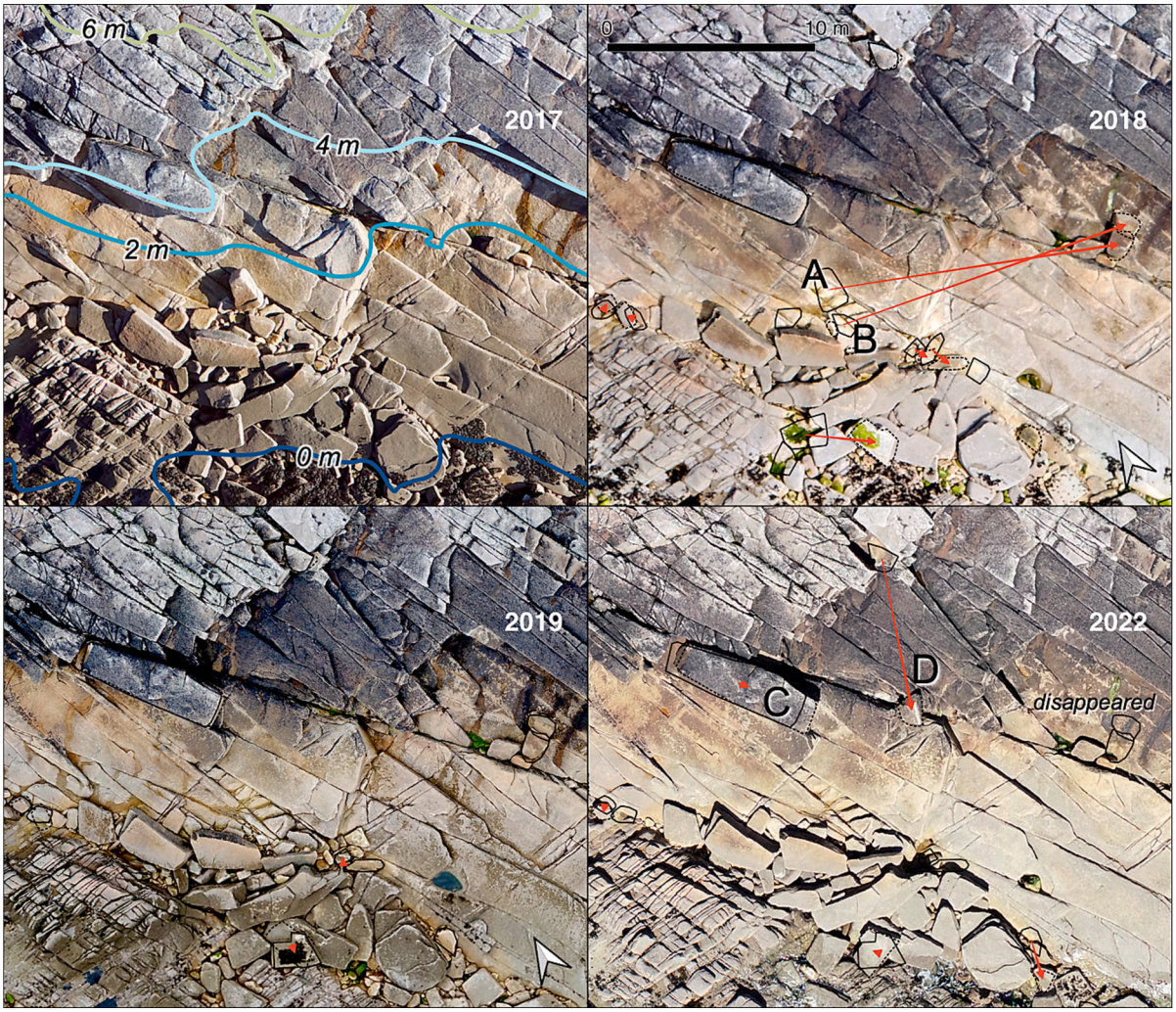


**Fig. 9.** Discrete boulder movement on the intertidal bedrock platform (indicated with red lines) from one time step to another. Boulder A is 2.27 $m^2$, and moves 14.14 m in between 2017 and 18, then does not move, but then disappears in 2019–22; Boulder B is 1.17 $m^2$ and followed the same behaviour moving 14.36 m to the east. Boulder C is 14.23 $m^2$ and shifted along the platform by 0.53 m between 2019 and 2022; Boulder D is 1.44 $m^2$ and moved 7.39 m between 2019 and 2022. Variations in platform biozonation that reflect intertidal position and platform weathering/erosion around this elevation are described by Burningham and Knight (2020).

changes observed across each time frame, but of varying magnitudes. One of the largest mobile boulders on the platform (boulder C in Fig. 9 which has an area of 14.23 $m^2$, with a volume likely approaching 4.5 $m^3$) is transported a short distance down the platform, whilst another (boulder D in Fig. 9, with an area of 1.44 $m^2$) appears to have been detached and is transported over 7 m seaward.

Associated with structurally-controlled channels, boulder movement is far more dynamic (Fig. 10). Here, at all the periods 2017–18, 2018–19 and 2019–22 there are complex and multidirectional movements by boulders in the main part of the channel depression, and constrained to within the steeper sides of the deepest part of the depression. This latter site is located at the seaward exit of the main channel itself, associated with changes in water velocity and with most vigorous wave and tidal movement into and out of the channel. This gives rise to the multidirectional patterns of boulder movements.

## 5. Discussion

Repeat UAV surveys and analysis using SfM photogrammetry show that the subsampled boulder populations are relatively mobile during the entire time period surveyed (September 2017–May 2022) and with respect to the different time slices examined (Table 1). Although there is variability in boulder behaviour in these time slices that reflect the interactions between wave run-up and the geomorphology of the shore platform (Figs. 5–7), there are also relatively consistent patterns of movement style (Table 1) which likely reflect the geological control on detached boulder morphology (see Knight and Burningham, 2011). The sites of boulder movement (Fig. 5) are also controlled by shoreline geomorphology, resulting in spatial differences in boulder concentration along the shoreline (Fig. 4) and capturing of boulders within structurally-controlled depocentres (Figs. 2, 3D, 10). A model describing these interrelationships is shown in Fig. 11. This highlights that not surprisingly there are feedbacks between wave-driven boulder movement and shoreline geomorphology but, as described earlier, this varies substantially along the shoreline with variations in mapped boulder density (Fig. 4).

An important point – and this is true of any such studies of boulder movement – is that surveys represent only a transient snapshot of boulder positions from which their dynamics (movement direction and magnitude between successive time periods) are then inferred. Real-time monitoring of boulder positions using air tags or similar is not feasible for periods longer than a few hours or for large numbers of boulders (e.g., Stephenson and Abazović, 2016; Eltner et al., 2017; Brayne et al., 2020), and thus repeat UAV surveys provide the best

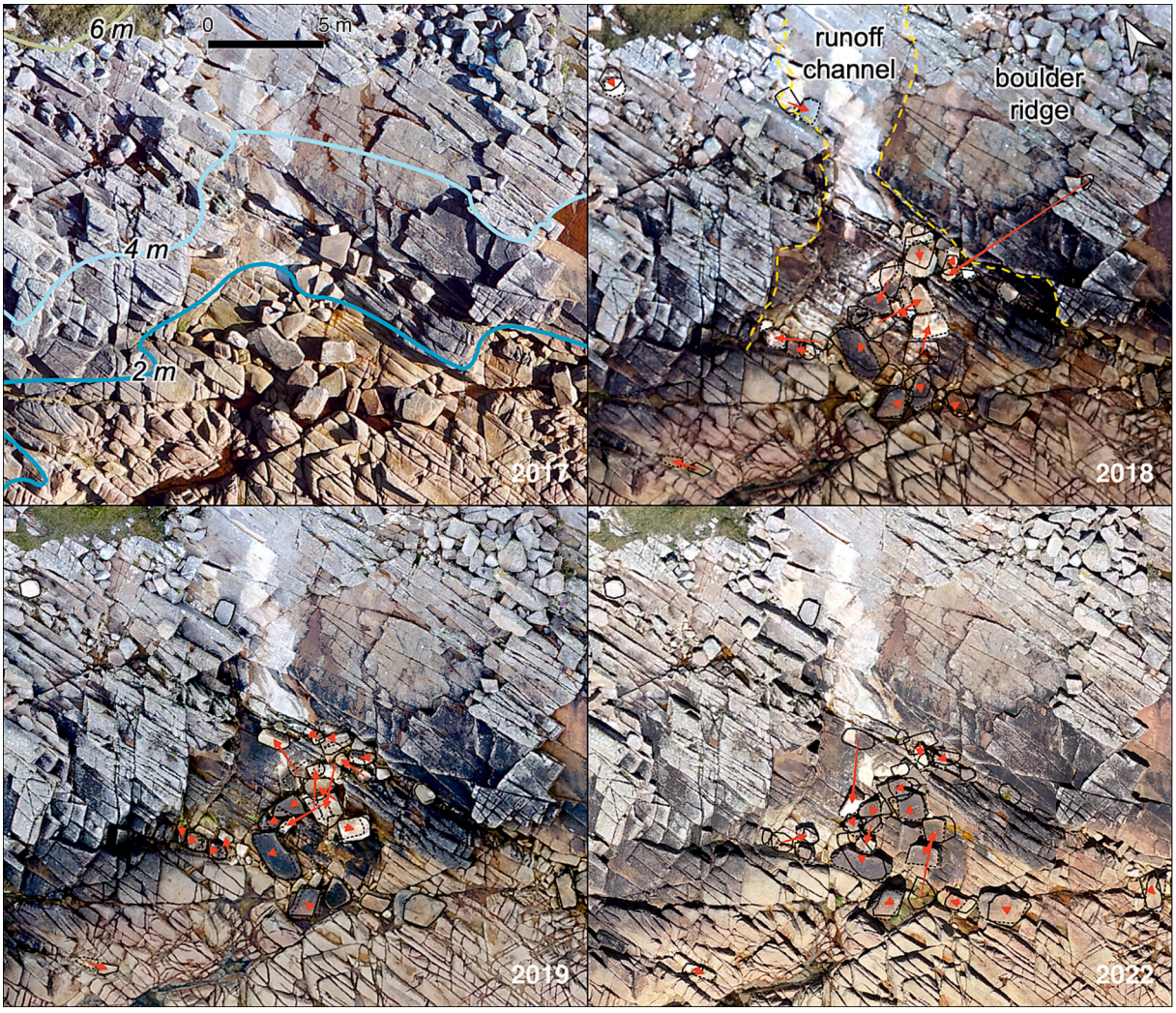


**Fig. 10.** Discrete boulder movement around a runoff channel from one time step to another. The margins of the channel are indicated in the yellow dotted line in the 2018 image. Boulder movements are indicated with red lines.

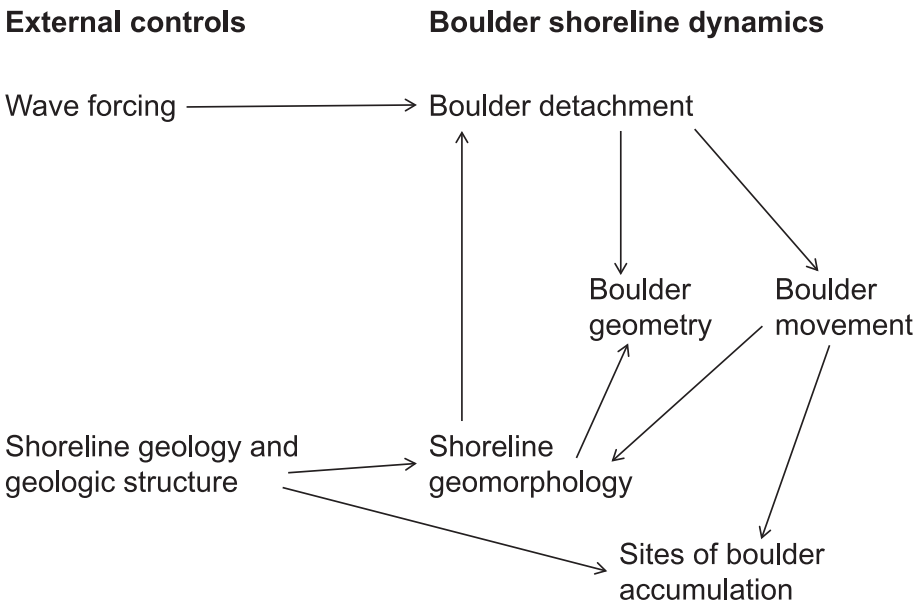


**Fig. 11.** Model of coastal boulder and shoreline dynamics in response to different external controls on their behaviour.

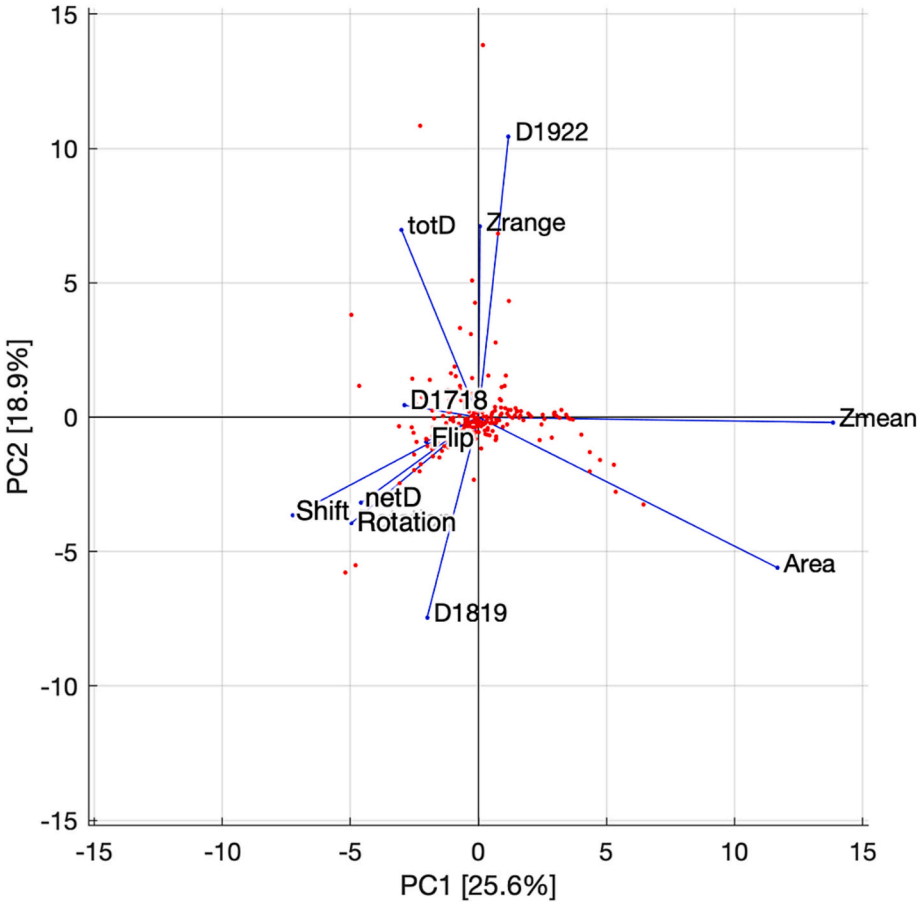


**Fig. 12.** PCA multivariate plot of mobile boulders that could be tracked across all temporal datasets. *D* is the distance moved in each period, *netD* is the net distance moved by the boulder whilst *totD* is the gross distance moved; *Zmean* is the average elevation, *Zrange* is the range of elevations experienced by the boulder in its journey; *area* and *elongation* capture boulder size/shape metrics; *Shift*, *Rotation* and *Flip* are pseudo- (Boolean) variables capturing the behaviour of each boulder in each time frame.

systematic and repeatable methodology for boulder mapping and analysis. The length of time between successive surveys has implications for the confidence in reconstruction of boulder dynamics, and this is a limitation of all such studies. As indicated above, only 55 % of boulders appear on all surveys across the 5-year time period, suggesting there is a relatively high turnover of boulder populations, supported by the relatively minor (but notable) proportion of boulders that appear and disappear aperiodically on the shoreline (Table 1). This has not been discussed in previous studies. This also highlights the 'serendipity' of occurrence of boulders observed at any one time, and that drawing conclusions uncritically about boulder transport and fluxes is problematic. Thus, boulder populations and their dynamics reflect a transient state of a rocky shoreline system, reflecting different forcings, responses, thresholds and quasi-stabilities. It should be noted that transience in environmental forcing–response relationships is an emerging theme in geomorphic research (e.g., Mudd, 2017; Knight and Harrison, 2018), and rocky shoreline dynamics should be considered in the same light.

### 5.1. Controls on boulder dynamics and implications for boulder transport by waves

Based on boulder movement data, multivariate principal components analysis (PCA) of boulders that could be identified across all surveys, and that travelled by at least 23 cm is shown in Fig. 12. The first two components explain <50 % of the total variance in the data, suggesting that other factors beyond those measured play an important role in the behaviour of these boulders. The clustering of data in the middle of the plot shows that for a large number of boulders, there are no clear properties that can explain their movements. Total distance travelled (*totD*) tends to be greater for smaller boulders (*Area*) and lower elevations (*Zmean*), and the net distance travelled (*netD*) increases with decrease in range of elevations (*Zrange*) crossed in the boulder's journey. The analysis implies that boulders moving larger distances in 2018–19 then moved shorter distances in 2019–22, and vice versa. Boulders that rotated tended to be associated with larger net distances travelled. However, these calculated measurements of straight-line distances between two observed boulder locations may not necessarily describe the actual transport paths undertaken by individual boulders.

The offshore wave climate during this monitoring period falls well within the recent envelope of variability over the last 40 years (Fig. 13), but monthly wave power peaked in the winter of 2021–22, and also reached a notable high in 2019–20. The total wave power experienced in each time period did vary, with both 2017–18 and 2018–19 experiencing lower power than that in 2019–22 (despite 2020–21 being a particular low power period). The maximum wave height in 2021–22 was 14.38 m, substantially greater than recent decades, but the associated 99th percentile of 8.48 m was equivalent to that during 2017–18 (8.43 m). The wave climate does little to help explain the range of different styles and directions of boulder movement that took place (Figs. 5–7). The larger distance outliers occurred in 2018–19, but the larger average distance took place during 2019–22 (Table 1), and the rationale that might explain a larger distance travelled does not then work for more boulders travelling or the average distance travelled being greater.

This lack of specific association between wave climate and specific characteristics of boulder motion is significant because most previous studies have focused exclusively on boulder movement under exceptional wave conditions related to large storms or tsunamis (e.g., Cox et al., 2018; Erdmann et al., 2018; Oliveira et al., 2020). These studies may therefore over-emphasise the role of these large wave events to the detriment of more 'average', normal or usual wave conditions under which it is likely that most boulder beaches and rocky shorelines

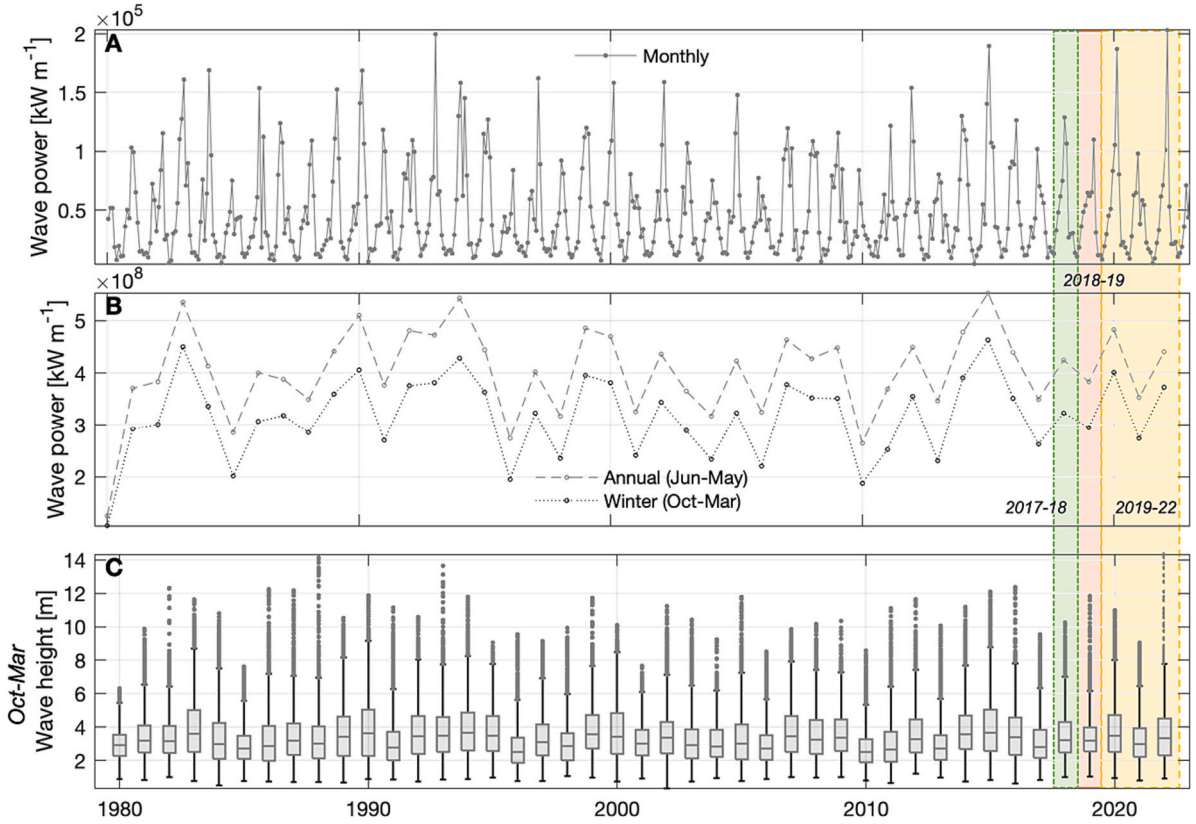


**Fig. 13.** Regional wave climate offshore northwest Ireland (ERA5 data for 55°N, 9°W) for the period 1980–2022, showing (A) monthly wave power, (B) annual (June to May) and winter (October to March) total wave power, and (C) winter (October to March) wave height distribution where the boxplots capture the median, interquartile range and outliers. The timings of the UAV surveys are shown by the shaded panels.

globally have evolved (e.g., Autret et al., 2018; Gómez-Pazo et al., 2019). It is also likely that the more subtle and diverse boulder movements that take place under 'average' or normal wave conditions, as described in this study, are likely masked or erased by the effects of extreme waves, which may mean there is low preservation potential of signatures of these average-state conditions (e.g., Barbano et al., 2010; Scheffers et al., 2012; Cox et al., 2019).

## 6. Conclusions

Repeated UAV surveys supported by analysis by SfM photogrammetry show that boulder positions and dynamics along the northwest Ireland coast are highly variable even when forced by 'average' or normal wave conditions. This highlights that rocky shoreline boulder movement does not take place only in association with large storms, which has been the dominant interpretation in the literature where large boulders have been moved inland and often to higher elevations (e.g., Cox et al., 2012; Erdmann et al., 2018). The survey data show that boulders are not equally distributed across the platform; they are quickly captured within hollows or fault-defined depressions on the platform surface or may exit the seaward end of depressions and so are lost from the system. This high turnover of shoreline boulders has not been considered in previous studies, where most emphasis has been on the static (relict) nature of boulder-dominated shorelines (e.g., Scheffers et al., 2012; Scheffers and Kinis, 2014; Erdmann et al., 2017). The greatest and most consistent patterns of boulder mobility take place on boulders on the platform surface with the smallest local relief, where boulders can more easily travel in any direction. There is also a high turnover of mapped boulders, with a relatively low proportion of boulders identified on successive surveys (Table 1). Boulders also appear/disappear from the spatial reference frame and in an inconsistent and somewhat chaotic manner.

This more nuanced understanding of boulder dynamics is significant for the interpretation of boulder beaches and rocky shorelines globally, where the previous emphasis on the role of extreme wave events may not necessarily describe the full spectrum of boulder behaviours, including transport, rotation, flipping, and appearance/disappearance. Understanding these different boulder behaviours is particularly important in light of global climate change where changes in wave climate as well as sea level are predicted (Siegert et al., 2020). This may result in a range of impacts on different types of boulder shorelines, according to shoreface steepness and lithology, as well as changes in $H_s$ and wave spectra (e.g., Naylor et al., 2016; Autret et al., 2018). In turn, this has implications for management applications and predictability of geomorphic change along coastlines. Thus, more intensive routine monitoring and analysis of boulder movements are required.

## Declaration of competing interest

The authors declare that they have no known competing financial interests or personal relationships that could have appeared to influence the work reported in this paper.

## Data availability

Data will be made available on request.

## Acknowledgements

We thank two anonymous reviewers for their comments on a previous version of this paper.

## References


Autret, R., Dodet, G., Fichaut, B., Suanez, S., David, L., Leckler, F., Ardhuin, F., Ammann, J., Grandjean, P., Allemand, P., Filipot, J., 2016. A comprehensive hydro-geomorphic study of cliff-top storm deposits on Banneg Island during winter 2013–2014. Mar. Geol. 382, 37–55.

Autret, R., Dodet, G., Fichaut, B., Suanez, S., David, L., Leckler, F., Ardhuin, F., Ammann, J., Grandjean, P., Allemand, P., Filipot, J.-F., 2018. A comprehensive hydro-geomorphic study of cliff-top storm deposits on Banneg Island during winter 2013–2014. Mar. Geol. 382, 37–55.

Autret, R., Didier, D., Suanez, S., Stéphan, P., Ammann, J., Baudry, J., Erlingsson, B., Sigurðarson, S., 2023. Cliff-top boulder morphodynamics on the high–energy volcanic rocky coast of the Reykjanes Peninsula (SW Iceland). Mar. Geol. 456, 106984 https://doi.org/10.1016/j.margeo.2022.106984.

Barbano, M., Pirrotta, C., Gerardi, F., 2010. Large boulders along the south-eastern Ionian coast of Sicily: storm or tsunami deposits? Mar. Geol. 275, 140–154.

Biolchi, S., Denamiel, C., Devoto, S., Korbar, T., Macovaz, V., Scicchitano, G., Vilibić, I., Furlani, S., 2019. Impact of the October 2018 Storm Vaia on Coastal Boulders in the Northern Adriatic Sea. Water 11, 2229. https://doi.org/10.3390/w11112229.

Boesl, F., Engel, M., Eco, R.C., Galang, J.B., Gonzalo, L.A., Llanes, F., Quix, E., Brückner, H., 2020. Digital mapping of coastal boulders – high-resolution data acquisition to infer past and recent transport dynamics. Sedimentology 67, 1393–1410.

Bonasera, M., Cerrone, C., Caso, F., Lanza, S., Fubelli, G., Randazzo, G., 2022. Geomorphological and Structural Assessment of the Coastal Area of Capo Faro Promontory, NE Salina (Aeolian Islands, Italy). Land 11, 1106. https://doi.org/10.3390/land11071106.

Brayne, R.P., Lorang, M.S., Naylor, L.A., Reinhardt, L., 2020. Field-based observation of the entrainment threshold of cobbles with motion loggers. J. Coast. Res. SI95, 392–397.

Bressan, L., Guerrero, M., Antonini, A., Petruzzelli, V., Archetti, R., Lamberti, A., Tinti, S., 2018. A laboratory experiment on the incipient motion of boulders by high-energy coastal flows. Earth Surf. Process. Landf. 43, 2935–2947.

Brunier, G., Fleury, J., Anthony, E.J., Gardel, A., Dussouillez, P., 2016. Close-range airborne Structure-from-Motion Photogrammetry for high-resolution beach morphometric surveys: examples from an embayed rotating beach. Geomorphology 261, 76–88.

Burningham, H., Knight, J., 2020. Biological zonation and bedrock strength on a high energy granite shore platform. J. Coast. Res. SI95, 23–28.

Carvalho, R.C., Reef, R., 2022. Quantification of coastal change and preliminary sediment budget calculation using SfM photogrammetry and archival aerial imagery. Geosciences 12, 357. https://doi.org/10.3390/geosciences12100357.

Carvalho, R.C., Kennedy, D.M., Niyazi, Y., Leach, C., Konlechner, T.M., Ierodiaconou, D., 2020. Structure-from-motion photogrammetry analysis of historical aerial photography: determining beach volumetric change over decadal scales. Earth Surf. Process. Landf. 45, 2540–2555.

Casella, E., Lewin, P., Ghilardi, M., Rovere, A., Bejarano, S., 2022. Assessing the relative accuracy of coral heights reconstructed from drones and structure from motion photogrammetry on coral reefs. Coral Reefs 41, 869–875.

Clark, A., Moorman, B., Whalen, D., Fraser, P., 2021. Arctic coastal erosion: UAV-SfM data collection strategies for planimetric and volumetric measurements. Arct. Sci. 7, 605–633.

Cooper, J.A.G., Green, A.N., Vital, H., Lima-Filho, F.P., 2019. Geomorphology and clast assemblages of intertidal beachrock: implications for submerged shoreline preservation. Geomorphology 343, 106–118.

Cox, R., Zentner, D.B., Kirchner, B.J., Cook, M., 2012. Boulder Ridges on the Aran Islands (Ireland): recent movements caused by storm waves, not tsunamis. J. Geol. 120, 249–272.

Cox, R., Jahn, K.L., Watkins, O.G., Cox, P., 2018. Extraordinary boulder transport by storm waves (west of Ireland, winter 2013–2014), and criteria for analysing coastal boulder deposits. Earth Sci. Rev. 177, 623–636.

Cox, R., O'Boyle, L., Cytrynbaum, J., 2019. Imbricated coastal boulder deposits are formed by storm waves, and can preserve a long-term storminess record. Sci. Rep. 9, 10784. https://doi.org/10.1038/s41598-019-47254-w.

Cox, R., Ardhuin, F., Dias, F., Autret, R., Beisiegel, N., Earlie, C.S., Herterich, J.G., Kennedy, A., Paris, R., Raby, A., Schmitt, P., Weiss, R., 2020. Systematic review shows that work done by storm waves can be misinterpreted as tsunami-related because commonly used hydrodynamic equations are flawed. Front. Mar. Sci. 7, 4. https://doi.org/10.3389/fmars.2020.00004.

Del Río, L., Posanski, D., Gracia, F.J., Pérez-Romero, A.M., 2020. A comparative approach of monitoring techniques to assess erosion processes on soft cliffs. Bull. Eng. Geol. Environ. 79, 1797–1814.

Delle Rose, M., Martano, P., Orlanducci, L., 2021. Coastal boulder dynamics inferred from multi-temporal satellite imagery, geological and meteorological investigations in Southern Apulia, Italy. Water 13, 2426. https://doi.org/10.3390/w13172426.

Eltner, A., Kaiser, A., Abellan, A., Schindewolf, M., 2017. Time lapse structure-from-motion photogrammetry for continuous geomorphic monitoring. Earth Surf. Process. Landf. 42, 2240–2253.

Erdmann, W., Kelletat, D., Kuckuck, M., 2017. Boulder ridges and washover features in Galway Bay, Western Ireland. J. Coast. Res. 33, 997–1021.

Erdmann, W., Kelletat, D., Scheffers, A., 2018. Boulder transport by storms – extreme-waves in the coastal zone of the Irish west coast. Mar. Geol. 399, 1–13.

Gallo, I.G., Martínez-Corbella, M., Sarro, R., Iovine, G., López-Vinielles, J., Hérnandez, M., Robustelli, G., Mateos, R.M., García-Davalillo, J.C., 2021. An Integration of UAV-based Photogrammetry and 3D modelling for rockfall hazard assessment: the Cárcavos case in 2018 (Spain). Remote Sens. 13, 3450 https://doi.org/10.3390/rs13173450.

Gómez-Pazo, A., Pérez-Alberti, A., Trenhaile, A., 2019. Recording inter-annual changes on a boulder beach in Galicia, NW Spain using an unmanned aerial vehicle. Earth Surf. Process. Landf. 44, 1004–1014.

Gómez-Pazo, A., Pérez-Alberti, A., Trenhaile, A., 2021. Tracking the behavior of rocky coastal cliffs in northwestern Spain. Environ. Earth Sci. 80, 757. https://doi.org/10.1007/s12665-021-09929-4.

Guisado-Pintado, E., Jackson, D.W.T., Rogers, D., 2019. 3D mapping efficacy of a drone and terrestrial laser scanner over a temperate beach-dune zone. Geomorphology 328, 157–172.

Hastie, W.W., Mthembu, A.T., Green, A.N., van den Bergh, J., 2021. Linking fracturing and rock mechanic properties to the erosion of a beachrock shore platform. Mar. Geol. 441, 106616 https://doi.org/10.1016/j.margeo.2021.106616.

Herterich, J.G., Cox, R., Dias, F., 2018. How does wave impact generate large boulders? Modelling hydraulic fracture of cliffs and shore platforms. Mar. Geol. 399, 34–46.

Knight, J., 2009. Subglacial erosion forms in northwest Ireland. Boreas 38, 545–554.

Knight, J., Burningham, H., 2011. Boulder dynamics on an Atlantic-facing rock coastline, northwest Ireland. Mar. Geol. 283, 56–65.

Knight, J., Harrison, S., 2018. Transience in cascading paraglacial systems. Land Degrad. Dev. 29, 1991–2001.

Knight, J., Burningham, H., Barrett-Mold, C., 2009. The geomorphology and controls on development of a boulder-strewn rock platform, NW Ireland. J. Coast. Res. SI56, 1646–1650.

Lin, Y.-C., Cheng, Y.-T., Zhou, T., Ravi, R., Hasheminasab, S.M., Flatt, J.E., Troy, C., Habib, A., 2019. Evaluation of UAV LiDAR for mapping coastal environments. Remote Sens. 11, 2893. https://doi.org/10.3390/rs11242893.

Long, C.B., McConnell, B.J., 1999. Geology of South Donegal: A Geological Description to Accompany the Bedrock Geology 1:100,000 Scale Map Series, Sheet 3 and Part of Sheet 4, South Donegal. Geological Survey of Ireland, Dublin, 116 pp.

Mancini, F., Dubbini, M., Gattelli, M., Stecchi, F., Fabbri, S., Gabbianelli, G., 2013. Using unmanned aerial vehicles (UAV) for high-resolution reconstruction of topography: the structure from motion approach on coastal environments. Remote Sens. 5, 6880–6898.

Minervino Amodio, A., Di Paola, G., Rosskopf, C.M., 2022. Monitoring coastal vulnerability by using DEMs based on UAV spatial data. ISPRS Int. J. Geo Inf. 11, 155. https://doi.org/10.3390/ijgi11030155.

Mudd, S.M., 2017. Detection of transience in eroding landscapes. Earth Surf. Process. Landf. 42, 24–41.

Nagle-McNaughton, T., Cox, R., 2020. Measuring change using quantitative differencing of repeat structure-from-motion photogrammetry: the effect of storms on coastal boulder deposits. Remote Sens. 12, 42. https://doi.org/10.3390/rs12010042.

Naylor, L.A., Stephenson, W.J., Smith, H.C.M., Way, O., Mendelssohn, J., Cowley, A., 2016. Geomorphological control on boulder transport and coastal erosion before, during and after an extreme extra-tropical cyclone. Earth Surf. Process. Landf. 41, 685–700.

Nott, J., 2003. Waves, coastal boulder deposits and the importance of the pre-transport setting. Earth Planet. Sci. Lett. 210, 269–276.

Oliveira, M.A., Scotto, M.G., Barbosa, S., de Andrade, C.F., da Conceição Freitas, M., 2020. Morphological controls and statistical modelling of boulder transport by extreme storms. Mar. Geol. 426, 106216 https://doi.org/10.1016/j.margeo.2020.106216.

Pagán, J.I., Bañón, L., López, I., Bañón, C., Aragonés, L., 2019. Monitoring the dune-beach system of Guardamar del Segura (Spain) using UAV, SfM and GIS techniques. Sci. Total Environ. 687, 1034–1045.

Papakonstantinou, A., Topouzelis, K., Pavlogeorgatos, G., 2016. Coastline Zones Identification and 3D Coastal Mapping Using UAV Spatial Data. ISPRS Int. J. Geo-Inf. 5 (75) https://doi.org/10.3390/ijgi5060075.

Pérez-Alberti, A., Trenhaile, A., 2015. An initial evaluation of drone-based monitoring of boulder beaches in Galicia, north-western Spain. Earth Surf. Process. Landf. 40, 105–111.

Rodarmel, C.A., Lee, M.P., Brodie, K.L., Spore, N.J., Bruder, B., 2019. Rigorous Error Modeling for sUAS Acquired Image-Derived Point Clouds. IEEE Trans. Geosci. Remote Sens. 57, 6240–6253.

Rowley, T., Ursic, M., Konsoer, K., Langendoen, E., Mutschler, M., Sampey, J., Pocwiardowski, P., 2020. Comparison of terrestrial lidar, SfM, and MBES resolution and accuracy for geomorphic analyses in physical systems that experience subaerial and subaqueous conditions. Geomorphology 355, 107056. https://doi.org/10.1016/j.geomorph.2020.107056.

Scheffers, A.M., Kinis, S., 2014. Stable imbrication and delicate/unstable settings in coastal boulder deposits: indicators for tsunami dislocation? Quat. Int. 332, 73–84.

Scheffers, A., Scheffers, S., Kelletat, D., Browne, T., 2009. Wave-emplaced coarse debris and megaclasts in Ireland and Scotland: boulder transport in a high-energy littoral environment. J. Geol. 117, 553–573.

Scheffers, A., Kelletat, D., Haslett, S., Scheffers, S., Browne, T., 2010. Coastal boulder deposits in Galway Bay and the Aran Islands, western Ireland. Z. Geomorphol. Suppl. 54, 247–279.

Scheffers, A.M., Scheffers, S.R., Kelletat, D.H., Squire, P., Collins, L., Feng, Y., Zhao, J.-X., Joannes-Boyau, R., May, S.M., Schellmann, G., Freeman, H., 2012. Coarse clast ridge sequences as suitable archives for past storm events? Case study on the Houtman Abrolhos, Western Australia. J. Quat. Sci. 27, 713–724.

Sedrati, M., Morales, J.A., El M'rini, A., Anthony, E.J., Bulot, G., Le Gall, R., Tadibaght, A., 2022. Using UAV and structure-from-motion photogrammetry for the detection of boulder movement by storms on a rocky shore platform in Laghdira, Northwest Morocco. Remote Sens. 14, 4102. https://doi.org/10.3390/rs14164102.

Siegert, M., Alley, R.B., Rignot, E., Englander, J., Corell, R., 2020. Twenty-first century sea-level rise could exceed IPCC projections for strong-warming futures. One Earth 3, 691–703.
Stephenson, W.J., Abazović, A., 2016. Measuring coastal boulder movement under waves using tri-axial accelerometers. J. Coast. Res. SI75, 607–611.
Stevenson, C., 2009. The relationship between forceful and passive emplacement: the interplay between tectonic strain and magma supply in the Rosses Granitic Complex, NW Ireland. J. Struct. Geol. 31, 270–287.
Stevenson, C.T.E., Hutton, D.H.W., Price, A.R., 2006. The Trawenagh Bay Granite and a new model for the emplacement of the Donegal Batholith. Trans. R. Soc. Edinb. Earth Sci. 97, 455–477.
Swirad, Z.M., Rosser, N.J., Brain, M.J., 2019. Identifying mechanisms of shore platform erosion using Structure-from-Motion (SfM) photogrammetry. Earth Surf. Process. Landf. 44, 1542–1558.
Van Blunk, A., Kennedy, A.B., Cox, R., 2021. Interplay between coastal elevation and wave height controls the occurrence of coastal boulder deposits in the Aran Islands, Ireland. Front. Earth Sci. 9, 715383 https://doi.org/10.3389/feart.2021.715383.
Warrick, J.A., Ritchie, A.C., Adelman, G., Adelman, K., Limber, P.W., 2017. New techniques to measure cliff change from historical oblique aerial photographs and Structure-from-Motion photogrammetry. J. Coast. Res. 33, 39–55.
Westoby, M.J., Brasingto, J., Glasser, N.F., Hambrey, M.J., Reynolds, J.M., 2012. 'Structure-from-Motion' photogrammetry: a low-cost, effective tool for geoscience applications. Geomorphology 179, 300–314.
Yao, Y., Burningham, H., Knight, J., Griffiths, D., 2023. Monitoring of coastal boulder movements by storms and calculating volumetric parameters using the volume differential method based on point cloud difference. Remote Sens. 15, 1526. https://doi.org/10.3390/rs15061526.
Yuan, R., Kennedy, D.M., Stephenson, W.J., Finlayson, B.L., 2022. The precision and accuracy of measuring micro-scale erosion on shore platforms. Mar. Geol. 443, 106691 https://doi.org/10.1016/j.margeo.2021.106691.
Zingg, T., 1935. Beitrag zur Schotteranalyse. Schweiz. Mineral. Petrogr. Mitt. 15, 39–140.